


## PAPER

View Article Online  
View Journal | View Issue

Cite this: *Biomater. Sci.*, 2024, **12**, 3947

# Diffusive delivery of plasmid DNA using zwitterionic carboxyalkyl poly(1-vinylimidazole) into skeletal muscle *in vivo*<sup>†</sup>

Ren Misaizu,<sup>a</sup> Yoko Endo-Takahashi,<sup>b</sup> Kei Nirasawa,<sup>b</sup> Yoichi Negishi<sup>b</sup> and Shoichiro Asayama  <sup>\*a</sup>

Zwitterionic carboxyalkyl poly(1-vinylimidazole) (CA-PVIm) polymers with imidazolium cations and carboxylate anions have been synthesized as a carrier for the *in vivo* delivery of plasmid DNA (pDNA) to skeletal muscle. From differential scanning calorimetry measurements, resulting CA-PVIm had intermediate water in hydration water as a biocompatible polymer. Notably, when the pDNA and resulting CA-PVIm were mixed, slight retarded bands of the pDNA were observed in agarose gel electrophoresis, suggesting the polyion complex (PIC) formation between the pDNA and CA-PVIm despite zwitterionic polymers. Resulting PICs maintained the higher-order structure of the pDNA. Using resulting pDNA PICs, the highest pDNA expression by intramuscular injection was achieved in the PIC with 7 mol% carboxymethylated PVIm, that is, CA<sub>1</sub>(7)-PVIm, observed in a widespread area by *in vivo* imaging system. These results suggest that the CA<sub>1</sub>(7)-PVIm/pDNA PIC is effective for the diffusive delivery of the pDNA into skeletal muscle for the treatment of serious muscle diseases.

Received 13th April 2024,  
Accepted 10th June 2024  
DOI: 10.1039/d4bm00510d  
rsc.li/biomaterials-science

## 1. Introduction

Since small interfering RNA (siRNA) capable of inducing RNA interference was reported in the early 2000s,<sup>1</sup> gene therapy using nucleic acid medicine has attracted attention as a next-generation medicine. Intramuscular injection of adenovirus (DNA) and messenger RNA (mRNA) vaccine for coronavirus disease 2019 (COVID-19) was widely carried out; therefore, skeletal muscle is an important target for gene delivery. Plasmid DNA (pDNA), a therapeutic gene, can produce therapeutic RNAs, such as the mRNA and non-coding RNA (ncRNA),<sup>2</sup> including siRNA, by transcription and therapeutic proteins by translation.<sup>3–5</sup> Generally, in clinical applications, gene expression from the pDNA is maintained *in vivo* and sustained production of the therapeutic RNAs and proteins is desired.<sup>6–8</sup> However, there are many barriers to the application of the pDNA as an effective medicine. First, the pDNA is an anionic polymer with a molecular weight exceeding 10<sup>6</sup> and thus cannot permeate cell membranes. Therefore, an entry

pathway *via* endocytosis is important, in which case endosomal escape is required to avoid degradation in late endosomes or lysosomes.<sup>9</sup> Furthermore, the pDNA is easily degraded by nucleases and is exposed to them immediately after local injection. Therefore, an effective drug delivery system (DDS) is needed to realize the clinical medicinal use of the pDNA. pDNA delivery systems widely use polyion complexes (PICs), which are based on electrostatic interactions between the pDNA and a cationic carrier. Many delivery systems using cationic polymers have been reported.<sup>2,10–13</sup> Especially for intramuscular gene delivery, carriers, such as lipid nanoparticles containing poly(ethylene glycol) (PEG) for mRNA vaccine<sup>14</sup> and the related pDNA delivery systems, have been reported.<sup>15–17</sup>

However, while cationic carriers promote gene delivery to cells, there are still issues, such as the formation of large aggregates *in vivo* and tendency to exhibit cytotoxicity due to the high positive charge on the particle surface.<sup>18</sup> The PICs formed by poly(L-lysine) or poly(ethyleneimine) have a particle size of approximately 100 nm in buffer solution, but after intravenous injection to mice, they were reported to form giant aggregates of micro-order by adsorption with blood cell components, such as platelets and serum albumin.<sup>19</sup> In PEGylation (PEG modification), the PIC surface is modified with PEG to inhibit nonspecific interactions; it is widely used in DDS because PEG is a nonionic, hydrophilic, and biocompatible material.<sup>20</sup> However, new issues have arisen, such as

<sup>a</sup>Department of Applied Chemistry, Tokyo Metropolitan University, 1-1 Minami-Osawa, Hachioji, Tokyo 192-0397, Japan. E-mail: asayama-shoichiro@tmu.ac.jp; Tel: +81426771111 (ext.): 4976

<sup>b</sup>School of Pharmacy, Tokyo University of Pharmacy and Life Sciences, 1432-1 Horinouchi, Hachioji, Tokyo 192-0392, Japan

<sup>†</sup>Electronic supplementary information (ESI) available. See DOI: <https://doi.org/10.1039/d4bm00510d>

inhibited cellular uptake into target cells and endosomal escape (PEG dilemma),<sup>21–23</sup> production of anti-PEG antibodies (ABC phenomenon),<sup>24–31</sup> and pseudo allergic reaction due to complement activation (CARPA).<sup>32</sup> Therefore, the zwitterionic polymers have recently attracted attention as an alternative material to PEG.<sup>33</sup> It has been reported that liposomes modified with poly(carboxybetaine) zwitterionic polymers do not produce anti-polymer antibodies, avoid the ABC phenomenon<sup>34</sup> and accumulate in the target tumour tissue.<sup>35</sup>

We have already designed two zwitterionic polymers, such as carboxymethyl poly(L-histidine) (CM-PLH)<sup>36,37</sup> and carboxymethyl poly(1-vinylimidazole) (CM-PVIm).<sup>38</sup> Ternary PICs formed reduced cytotoxicity and had comparable or better gene expression *in vitro* and *in vivo*<sup>39,40</sup> compared to binary PICs. Both the zwitterionic polymers have the imidazolium cations as cationic moiety and unmodified (imidazolium-free) imidazole groups to impart a proton sponge effect and endosomal escape. We also chose a ternary PIC to coat the surface of the PEI/pDNA binary PIC by non-covalent bonding (electrostatic interaction), instead of covalent modification, such as PEGylation. Ternary PICs formed show reduced cytotoxicity and a comparable or better gene expression *in vitro* and *in vivo* compared to the binary PICs. As far as we know, while there are few reports of binary pDNA PICs with ammonium-based zwitterionic polymers,<sup>41,42</sup> there are no reports on the binary pDNA PICs with imidazolium-based zwitterionic polymers.

Here, imidazolium cation is expected to form stronger non-covalent bonds, such as electrostatic interactions and  $\pi$ - $\pi$  interactions, than other ammonium cations, because the positive charge of the imidazolium cation is delocalized in the five-membered heterocycle.<sup>43</sup> Furthermore, higher transfection efficiency and reduced cytotoxicity of the PICs based on imidazolium-DNA interaction have been reported as compared with the PICs based on quaternary ammonium-DNA interaction.<sup>44,45</sup> Therefore, the zwitterionic polymers alone may be able to replace the carrier design of the cationic carriers with biocompatible polymers that have been considered so far. Based on our previous report, these backgrounds have led us to design an original zwitterionic polymer and a carboxyalkyl poly(1-vinylimidazole) (CA-PVIm), which is a linkage between an imidazolium cation and a carboxylate anion.<sup>38</sup> Not the zwitterionic polymers alone, but block copolymers with a zwitterionic block and cationic block may be useful for the PICs, such as liposomes modified with the zwitterionic polymers. However, the cationic block (polycation) has the destiny to exhibit potential cytotoxicity. Instead of using the CA-PVIm for surface modification of complexes, such as liposomes, we used the CA-PVIm alone as a carrier to form the PICs in this study.

## 2. Materials and methods

### 2.1. Materials

1-Vinylimidazole (VIm) was purchased from Tokyo Chemical Industry Co., Ltd (TCI). 2,2'-Azobis(isobutyronitrile) (AIBN) was

purchased from Sigma-Aldrich. Iodoacetic acid and Nile red were purchased from Wako Pure Chemical Industries. 3-Iodopropionic acid, 3-bromopropionic acid, 5-bromovaleric acid, 6-bromohexanoic acid and 8-bromooctanoic acid were purchased from TCI. *N,N*-Dimethylformamide (DMF) was purchased from Kanto Chemical Co., Inc. Dimethyl sulfoxide (DMSO) was purchased from Wako Pure Chemical Industries. All other chemicals of special grade were used without further purification.

### 2.2. Synthesis of CA-PVIm zwitterionic polymers

The CA-PVIm zwitterionic polymers were synthesized according to our previous paper.<sup>34</sup> Each CA-PVIm was synthesized by mixing PVIm with each  $\omega$ -bromocarboxylic acid and  $\omega$ -iodocarboxylic acid in DMF or DMSO, depending on the length of the alkyl chain.

### 2.3. Gel filtration chromatography (GFC)

GFC was carried out using a JASCO PU-980 pumping system (Tokyo, Japan) at a flow rate of 1.0 mL min<sup>-1</sup> with a Shodex OHPak SB-804 HQ column (Showa Denko K.K., Tokyo, Japan). The aqueous solution containing 0.5 M CH<sub>3</sub>COOH and 0.2 M NaNO<sub>3</sub> was used as a mobile phase. Eluate was analysed by a refractive index detector (RI-1530, JASCO). Calibration was performed with polyethylene glycol standards.

### 2.4. <sup>1</sup>H NMR spectroscopy

The resulting polymer (3 mg) was dissolved in 500  $\mu$ L of DMSO-*d*<sub>6</sub> (99.9 atom % deuterium; Acros, NJ) and 100  $\mu$ L of trifluoroacetic acid. <sup>1</sup>H NMR spectra (500 MHz) were obtained on a Bruker AV500 spectrometer (Billerica, MA).

### 2.5. Critical aggregation concentration (CAC) measurement

A Nile red stock solution (0.2 mg mL<sup>-1</sup>) with acetone was prepared, and 10  $\mu$ L of the solution was added to the vial. Then, CA-PVIm stock solutions in PBS(-) with various concentrations were prepared and added to the vial, followed by incubation at 37 °C for 1 h. Fluorescence intensity was measured from 580 nm to 720 nm (excitation wavelength: 550 nm) using a spectrofluorometer.

### 2.6. Differential scanning calorimetry (DSC) measurement

DSC was carried out using a HITACHI DSC-7000X. CA-PVIm/water samples with various water contents were prepared according to the following procedure. Each CA-PVIm (4.20 mg) and various amounts of water (about 50 wt%) were mixed and stored at 37 °C in pans. At this time, we also weighed the sample before adding water. Then, we determined the exact weight of water by weighing the samples after adding water. For the DSC measurement, the samples were cooled to -100 °C at a cooling rate of 10 °C min<sup>-1</sup>. Subsequently, resulting samples were heated to 50 °C at a heating rate of 10 °C min<sup>-1</sup>. During measurements, nitrogen gas was passed with a flow rate of 20 mL min<sup>-1</sup>.

## 2.7. Hemolysis assay

The stock solution (1 mg mL<sup>-1</sup>) of the CA-PVIm was prepared with 20 mM phosphate buffer (pH 7.4 or 5.1) containing 130 mM NaCl. Then, 40 µL of the CA-PVIm stock solution was incubated with 20 µL mouse preserved blood for 3 h at 37 °C. After centrifugation (13 200 rpm, 10 min, 4 °C), the amount of haemoglobin released was determined by measuring the absorbance of 5-fold diluted supernatant at 570 nm.

## 2.8. Agarose gel retardation assay

A stock solution of the CA-PVIm and dilution (300 ng of pDNA) of pDNA stock solution with PBS(-) were mixed where the final volume was adjusted to 13.5 µL at various [Im<sup>+</sup>]<sub>CA-PVIm</sub>/[R<sub>2</sub>PO<sub>4</sub><sup>-</sup>]<sub>pDNA</sub> ratios, followed by the incubation at 37 °C for 1 h. After mixing with a loading buffer (1.5 µL), the resulting sample was loaded onto a 1% agarose gel containing 1 µg mL<sup>-1</sup> ethidium bromide. Gel electrophoresis (50 V, 30 min) was performed at room temperature in a TAE buffer (Tris-acetate, EDTA, pH 8.3) or phosphate buffer solution (NaH<sub>2</sub>PO<sub>4</sub>, Na<sub>2</sub>HPO<sub>4</sub>, pH 6.0), followed by the visualization of pDNA bands under UV irradiation by a gel documentation system (GelDoc Go, BIO-RAD).

## 2.9. Particle size and zeta (ζ) potential measurement

A dynamic light scattering (DLS) method by an electrophoresis light scattering (ELS) spectrophotometer (ELS-Z2, Otsuka Electronics Co., Ltd) determined the size of the pDNA (5 µg) incubated at 37 °C for 1 h with the CA-PVIm at various [Im<sup>+</sup>]<sub>CA-PVIm</sub>/[R<sub>2</sub>PO<sub>4</sub><sup>-</sup>]<sub>pDNA</sub> ratios in 100 µL of phosphate-buffered saline, PBS(-). The ζ-potential of the resulting sample was measured by ELS with electrodes.

## 2.10. Observation of the PIC morphology by transmission electron microscopy (TEM)

Initially, two microliters of PIC solution with 2 µL of 2% uranyl acetate on ice were used for a TEM sample solution to observe the resulting PICs. After a TEM grid (Nisshin EM Co., Tokyo, Japan) was hydrophilized by an Eiko IB-3 ion coater (Eiko Engineering Co., Ltd, Simane, Japan), the hydrophilized grid was dipped into the sample solution for 40 s. The excess solution was blotted away. The observation of resulting grids was carried out by a JEM-1400 Bio-TEM (JEOL Ltd, Tokyo, Japan) operated at an acceleration voltage of 120 kV.

## 2.11. Circular dichroism (CD) spectrum measurement

For the PIC formation, pDNA (5 µg) was incubated at 37 °C for 1 h with each CA-PVIm at a [Im<sup>+</sup>]<sub>CA-PVIm</sub>/[R<sub>2</sub>PO<sub>4</sub><sup>-</sup>]<sub>pDNA</sub> ratio of 64. After the PICs were formed, the solution volume was adjusted to 350 µL with PBS(-). The CD spectrum was measured from 240 nm to 320 nm with a circular dichroism spectropolarimeter (J-820, JASCO Co., Ltd, Tokyo, Japan).

## 2.12. Cell viability assay

As a representative cell, mouse myoblast cell line C2C12 cells (from Riken Bioresource Center Cell Bank) were cultured in

tissue culture flasks in Dulbecco's modified Eagle's medium supplemented with 10% heat-inactivated FBS. The cells were seeded at 1 × 10<sup>4</sup> cells per well in a 96-well plate, followed by incubation overnight at 37 °C in a 5% CO<sub>2</sub> incubator. The cells were then treated with each CA-PVIm, followed by further incubation for 24 h at 37 °C. By additional incubation for 4 h, the cell viability was measured by the Alamar Blue assay<sup>46</sup> in triplicate.

## 2.13. *In vivo* gene delivery to the skeletal muscle

*In vivo* gene delivery to the skeletal muscles of mice with each CA-PVIm was carried out using previously described methods.<sup>47</sup> Briefly, ICR mice (five weeks old, male) were anaesthetized with pentobarbital. The PICs of the pDNA (5 µg) with each CA-PVIm at the [Im<sup>+</sup>]<sub>CA-PVIm</sub>/[R<sub>2</sub>PO<sub>4</sub><sup>-</sup>]<sub>pDNA</sub> ratios of 64 in 35 µL of PBS(-) were incubated at 37 °C for 1 h, followed by injection into the tibialis muscles of the ICR mice. One week after the injection, the whole tibialis muscles were collected and homogenized in a lysis buffer (0.1 M Tris-HCl: pH 7.8, 0.1% Triton X-100, and 2 mM EDTA). Luciferase activity was measured with a luminometer (LB96 V, Berthold Japan Co. Ltd, Tokyo, Japan) according to a luciferase assay system (Promega, Madison, WI, USA). The luciferase activity is normalized by relative light units (RLU) per mg of protein. The pcDNA3-Luc plasmid was derived from pGL3-basic (Promega, Madison, WI, USA) and used as a pDNA encoding the firefly luciferase gene under the control of a cytomegalovirus promoter.

## 2.14. *In vivo* gene delivery to the skeletal muscle

Luciferase gene expression was observed using an *in vivo* imaging system (IVIS Lumina Series III, PerkinElmer, Waltham, USA) for one week. During the measurement, VivoGro Luciferin (Promega; 10 µg per mg body weight) was administered intraperitoneally; the samples were incubated for 10 min before observation.

## 2.15. Animals

The use of animals and relevant experimental procedures were approved by the Tokyo University of Pharmacy and Life Science Committee on the Care and Use of Laboratory Animals.

## 2.16. Statistical analysis

Statistical analysis was performed using the two-sample equal variance student's *t*-test.

# 3. Results and discussion

## 3.1. Synthesis of the CA-PVIm zwitterionic polymers

The synthetic scheme of the CA-PVIm zwitterionic polymers is shown in Fig. 1. The number-average molecular weight (*M<sub>n</sub>*) of the PVIm backbone was estimated to be 3.8 × 10<sup>3</sup> (*M<sub>w</sub>*/*M<sub>n</sub>* = 2.2, DP = 40) by GFC (Fig. S1†). The <sup>1</sup>H NMR spectra of resulting representative polymers show the characteristic signal of imidazole groups, which exhibit a down-field shift after the

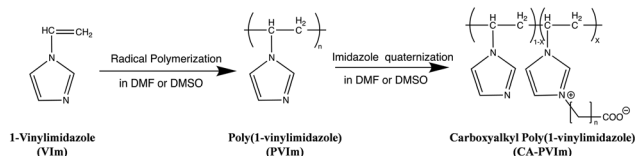


Fig. 1 Synthesis scheme of the CA-PVIm zwitterionic polymers.

reaction, confirming the progress of the carboxy-alkylation of the imidazole groups (Fig. S2†). The degree of modification of CA groups was calculated from the integrals of signals derived from the methylene chains of the CA groups against each CA-PVIm backbone signal. In this study, each CA-PVIm is denoted according to its structure (Table 1).

### 3.2. Physicochemical properties of the CA-PVIm zwitterionic polymers

From the viewpoint of biocompatibility assessed by physicochemical properties, it has been reported that biocompatible polymers, such as poly(2-methoxyethylacrylate) (PMEA) exhibit excellent biocompatibility by retaining intermediate water in hydration water.<sup>48</sup> In this report, according to DSC analysis, freeze-bound water (intermediate water<sup>49</sup>) is the water that exhibits low-temperature crystallization at around  $-40^{\circ}\text{C}$  during the temperature increase due to its amorphous structure in polymers. In the case of the zwitterionic poly(2-methacryloyloxyethyl phosphorylcholine) (PMPC)-water system,<sup>50</sup> it is known that two endothermic peaks are observed below  $0^{\circ}\text{C}$ , and low-temperature crystallization is observed as a broad exothermic peak in the heating process. In this study, DSC curves were obtained for the various CA-PVIm zwitterionic polymers during the heating process (Fig. S3†). In addition to two endothermic peaks around  $-20^{\circ}\text{C}$ , a broad exothermic peak was observed around  $-50^{\circ}\text{C}$ . Therefore, we conclude that the CA-PVIm zwitterionic polymers retain the intermediate water in the hydration water because the DSC curve of the CA-PVIm-water system was very similar to that of the PMPC-water system. Furthermore, although a similar behaviour was always observed even in highly concentrated aqueous solutions of inorganic salts, the dependence of resulting DSC curves on the methylene spacer length between zwitterionic groups supports the existence of the intermediate water.

From the viewpoint of the effect of the assembling structure on biocompatibility, the PIC formation by electrostatic inter-

action between the CA-PVIm zwitterionic polymers may occur to form a hydrophobic environment because CA-PVIm has positive and negative charges per monomer unit. Furthermore, the long methylene chains of CA<sub>7</sub>-PVIm may form another hydrophobic environment. Therefore, we checked whether the CA-PVIm zwitterionic polymers form a hydrophobic environment by estimating the critical aggregation concentration (CAC). The negligible CAC confirmed that CA<sub>1</sub>-PVIm and CA<sub>7</sub>-PVIm did not form a hydrophobic environment (Fig. S4†).

### 3.3. Biochemical properties of the CA-PVIm zwitterionic polymers

The potential toxicity of the polymers as pDNA carriers to the cells is an important consideration for clinical applications. Free polymers are only present when the pDNA is released from the PIC. Furthermore, the cytotoxicity of the free polymer is likely to be higher than that of the core PIC. Therefore, we performed cytotoxicity assays of the free polymers to give a worst-case scenario of polymer-cell interaction rather than PIC-cell interaction; the effect of each CA-PVIm on cell viability in C2C12 mouse myoblasts is shown in Fig. 2. The branched polycation and branched poly(ethylenimine) (bPEI) significantly reduced cell viability, whereas unmodified PVIm exhibited no apparent cytotoxicity (Fig. S5†). Conversely, the CA-PVIm zwitterionic polymers maintained a high cell viability of almost 100%, regardless of the degree of modification of the carboxyalkyl. These results can be attributed to the negligible accessibility of the zwitterionic groups to cell membranes because the bPEI and unmodified PVIm did not possess the intermediate water (Fig. S6†). Conversely, cationic groups on the bPEI were easily accessible to anionic cell membranes and disturbed the membranes. Namely, the CA-PVIm with a zwitterionic group showed a negative charge repulsion with anionic cell membranes, due to the presence of an anionic carboxyl group outside the cationic imidazolium group.

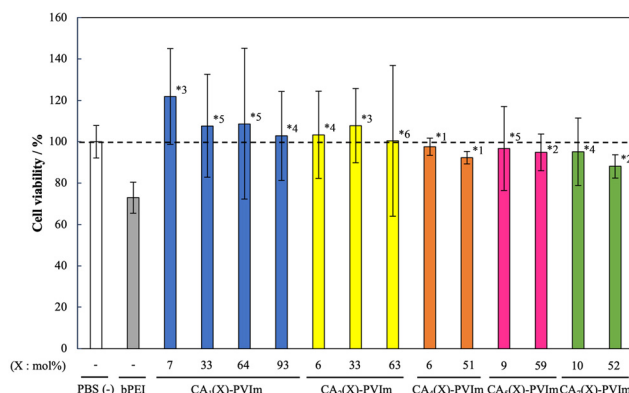


Fig. 2 Effect of the CA-PVIm on cell (C2C12) viability. Symbols and error bars represent the mean and standard deviation of the measurements made in quintuplicate wells. \* indicates statistical significance when compared to the bPEI (\*1,  $p < 0.0001$ ; \*2,  $p < 0.001$ ; \*3,  $p < 0.005$ ; \*4,  $p < 0.01$ ; \*5,  $p < 0.05$ ; and \*6,  $p < 0.1$ ). The concentrations of the CA-PVIm are  $0.9\text{--}9.8\text{ mg mL}^{-1}$  with same molar CA groups.

Table 1 Abbreviation of each CA-PVIm zwitterionic polymers

Methylene chain length	CA structure	Abbreviation *X : CA modification degree/ mol%
1	Carboxy methyl	CA <sub>1</sub> (X)-PVIm
2	Carboxy ethyl	CA <sub>2</sub> (X)-PVIm
4	Carboxy butyl	CA <sub>4</sub> (X)-PVIm
5	Carboxy pentyl	CA <sub>5</sub> (X)-PVIm
7	Carboxy heptyl	CA <sub>7</sub> (X)-PVIm



Especially, when the PICs between the CA-PVIm and pDNA were formed, anionic carboxyl groups outside cationic imidazole groups were considered advantageous for such an orientation in the PICs. Furthermore, although the anti-PEG antibody response is now under investigation for further biocompatibility, the body weight of the mouse injected with the CA-PVIm was five times and did not decrease for 35 days (results not shown), as compared to that without the CA-PVIm. This observation suggests no side effects, such as antibody response.

### 3.4. Biochemical properties of the CA-PVIm zwitterionic polymers

As shown in Fig. 3, the PIC formation of the various CA-PVIm zwitterionic polymers with the pDNA was evaluated by agarose gel electrophoresis. The mixing charge ratios of the imidazolium group of the CA-PVIm to the phosphate group of pDNA,  $[Im^+]_{CA-PVIm}/[R_2PO_4^-]_{pDNA}$ , were evaluated from 0.5 to 256. As a result, each CA-PVIm seems to exhibit no significant difference in the electrophoresis pattern. Especially, the increase in the quaternization degree of each CA-PVIm seems to retard the migration of the pDNA band at the same  $[Im^+]_{CA-PVIm}/[R_2PO_4^-]_{pDNA}$  ratio, suggesting the dependence of the CA-PVIm/pDNA PIC formation on the quaternization degree. Notably, each CA-PVIm is zwitterionic; nevertheless, the retardation of the naked pDNA-derived band was observed to be above the  $[Im^+]_{CA-PVIm}/[R_2PO_4^-]_{pDNA}$  ratio of 8 in most samples, suggesting PIC formation. Furthermore, complete PIC formation with no band of naked pDNA was observed above the  $[Im^+]_{CA-PVIm}/[R_2PO_4^-]_{pDNA}$  ratio of 64, which was considered to be an optimum charge ratio in all CA-PVIm zwitterionic polymers. These results suggest that concentrated conditions are necessary to form CA-PVIm/pDNA PICs because of the less accessibility to the imidazolium cations due to the zwitterionic property of the CA-PVIm. Resulting retarded bands exhibited

significant fluorescence due to ethidium bromide staining, suggesting less condensation of the pDNA in these PICs.<sup>51</sup>

It should be noted that a band with a strong increase in migration over the naked pDNA was observed. Resulting “hyper-electrophoresis” bands were also observed without the pDNA (Fig. S7†), suggesting free CA-PVIm zwitterionic polymers. The migration was enhanced, when the modification degree and methylene chain length of the CA groups increased, suggesting the formation of small particles with anionic surface by each CA-PVIm zwitterionic polymer alone. Indeed, each CA-PVIm exhibited small particle sizes (Fig. S8A†) and negative  $\zeta$ -potentials (Fig. S8B†) despite the presence of the imidazolium cations to form assemblies. This could presumably be due to intermolecular electrostatic interactions without a hydrophobic environment (Fig. S4†). Therefore, although details are now under investigation as basic science, from a practical viewpoint, the “hyper-electrophoresis” can purify resulting CA-PVIm/pDNA PICs, because the PIC formation is not an equilibrium reaction to disintegrate.

### 3.5. Characterization of the CA-PVIm/pDNA PICs

The particle sizes and  $\zeta$ -potentials of the resulting CA-PVIm/pDNA PICs in PBS(−) are shown in Fig. 4A and B, respectively, with a polydispersity index (Table S1†) at a  $[Im^+]_{CA-PVIm}/[R_2PO_4^-]_{pDNA}$  ratio of 64 because of no free naked pDNA. The shorter bar of each particle size (Fig. 4A) is considered a free CA-PVIm zwitterionic polymer that exhibits the above-mentioned (Fig. S7†) hyper-electrophoresis. Representative scattering intensity distribution suggests that the fraction of the small particle size, which was considered to be free CA-PVIm alone, was approximately 30% of the total (Fig. S9†). Conversely, the longer bar of each particle size (Fig. 4A) is associated with the CA-PVIm/pDNA PIC, which was supported by the morphology observed by representative TEM images (Fig. S10†).

Resulting higher  $\zeta$ -potentials as compared to the potential of the naked pDNA to support PIC formation between the pDNA and each CM-PVIm, despite the formation of the zwitterionic polymer. Especially, the  $\zeta$ -potentials (Fig. 4B) of the CA<sub>1</sub>-PVIm/pDNA PICs were approximately −10 mV. The resulting  $\zeta$ -potentials were between the  $\zeta$ -potentials of the naked pDNA (approximately −35 mV: Fig. 4B) and CA<sub>1</sub>-PVIm

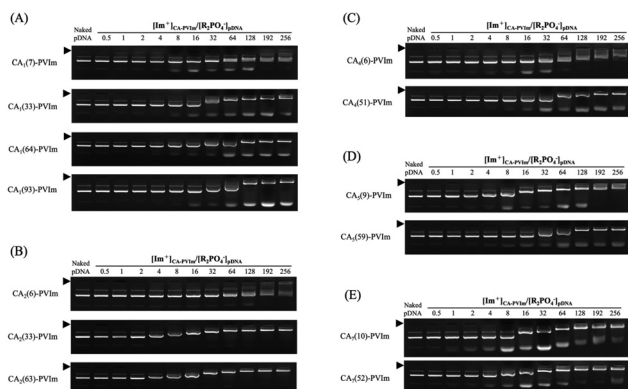


**Fig. 3** Analysis for the pDNA PIC formation with each CA-PVIm by agarose gel electrophoresis: (A) CA<sub>1</sub>-PVIm, (B) CA<sub>2</sub>-PVIm, (C) CA<sub>4</sub>-PVIm, (D) CA<sub>5</sub>-PVIm, and (E) CA<sub>7</sub>-PVIm. The mixing charge ratios of the imidazolium group of the CA-PVIm to the phosphate group of the pDNA are indicated as  $[Im^+]_{CA-PVIm}/[R_2PO_4^-]_{pDNA}$ . The solid arrowhead indicates the well where each sample was loaded.

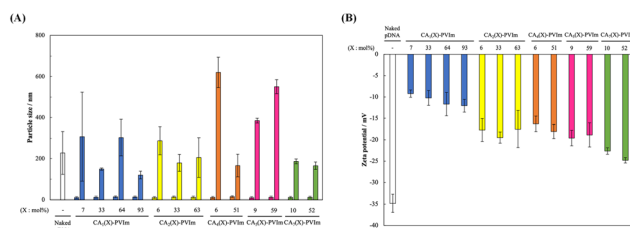


**Fig. 4** Particle size and  $\zeta$ -potential of the CA-PVIm/pDNA PICs: (A) Particle size and (B)  $\zeta$ -potential. The mixing charge ratios,  $[Im^+]_{CA-PVIm}/[R_2PO_4^-]_{pDNA}$ , are 64.

alone (approximately  $-6$  mV; Fig. S8B†). These results suggest that the PIC formation between the anionic phosphate group of pDNA and the cationic imidazolium group of the CA<sub>1</sub>-PVIm liberates the anionic carboxyl group of the CA<sub>1</sub>-PVIm. Furthermore, it should be noted that the  $\zeta$ -potentials (Fig. 4B) of the CA<sub>1</sub>-PVIm/pDNA PICs were weaker (approximately  $-10$  mV) than those of other PICs (approximately  $-20$  mV). It has been reported that the interaction between zwitterionic charged groups of a carboxybetaine molecule decreases drastically as the length of the methylene chain exceeds 2.<sup>52</sup> Therefore, in the case of carboxyalkyl imidazolium groups in the CA-PVIm zwitterionic polymers, the difference in the strength of the charge of the carboxylate anion, due to the difference in the length of the methylene chain, may decrease the negative  $\zeta$ -potentials on the surface of the CA<sub>1</sub>-PVIm/pDNA PICs.

To examine the higher-order structure of the pDNA in the resulting PICs, we measured the CD spectra of the PICs. In general, as shown in Fig. 5 (as well as Fig. S11†), the pDNA exhibits characteristic peaks derived from the B-type double helical structure, including a negative peak around 250 nm and positive peak around 280 nm. The resulting CD spectra of all the CA-PVIm/pDNA PICs were similar to the spectrum of the naked pDNA, suggesting that the higher-order structure of the pDNA was preserved.

### 3.6. Gene expression by the CA-PVIm/pDNA PICs *in vivo*

Finally, pDNA gene expression was evaluated by intra-muscular injection without *in vitro* evaluation because our previous report proved the noncorrelation between *in vitro* and *in vivo* conditions for pDNA transfection by intra-muscular injection.<sup>53</sup> After the injection of the CA-PVIm/pDNA PICs, there was no change in the health status of the mice or appearance of the injection site. Conversely, when the *in vivo* transfection reagent PEI (commercially available *in vivo*-jet-PEI™) was injected, white aggregation was observed at the site of the

injection (results not shown). These results suggest the better biocompatibility of the CA-PVIm zwitterionic polymer and less biocompatibility of the PEI cationic polymer to cause nonspecific interaction with anionic serum proteins. For intramuscular injection, the naked pDNA was used in several clinical trials to mediate significant gene expression<sup>54,55</sup> and was first approved in Japan in 2019. Fig. 6A shows the results of the gene expression mediated by the CA-PVIm/pDNA PICs in mouse skeletal muscles. In this *in vivo* experiment for the gene expression of the pDNA, the mixing charge ratio ( $[Im^+]_{CA-PVIm}/[R_2PO_4^-]_{pDNA}$ ) of 64 was selected because no free naked pDNA existed in the CA-PVIm/pDNA PICs (Fig. 3). The CA-PVIm/pDNA PICs with lower degree of CA group modification presented higher gene expression than the naked pDNA during clinical use, although the unmodified PVIm and naked pDNA did not form the PICs under experimental conditions in this study (Fig. S12†).

The resulting gene expression decreased, when the degree of modification of the CA group of each CA-PVIm increased, presumably due to the increased biocompatibility of more dense CA groups to form zwitterions. Specifically, the improved biocompatibility resulted in a reduction in the amount of the pDNA that could be transported and thus a reduction in gene expression. The resulting gene expression

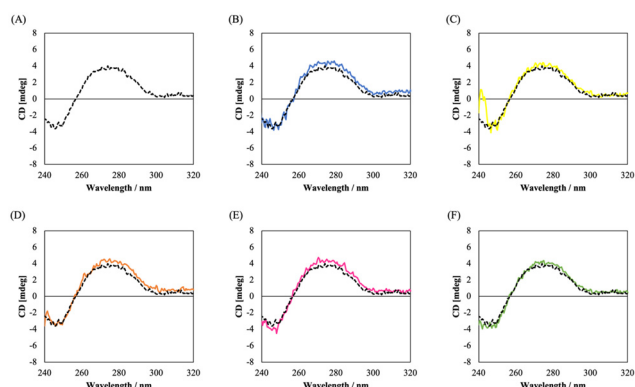


**Fig. 5** CD spectra of the (A) naked pDNA and PICs between the pDNA and CA-PVIm zwitterionic polymers with lower CA modification degree, such as (B) CA<sub>2</sub>(7)-PVIm, (C) CA<sub>2</sub>(6)-PVIm, (D) CA<sub>4</sub>(6)-PVIm, (E) CA<sub>5</sub>(9)-PVIm, and (F) CA<sub>7</sub>(10)-PVIm. The mixing charge ratios,  $[Im^+]_{CA-PVIm}/[R_2PO_4^-]_{pDNA}$ , are 64. The CD spectrum of the naked pDNA is represented as black dotted line in each panel.

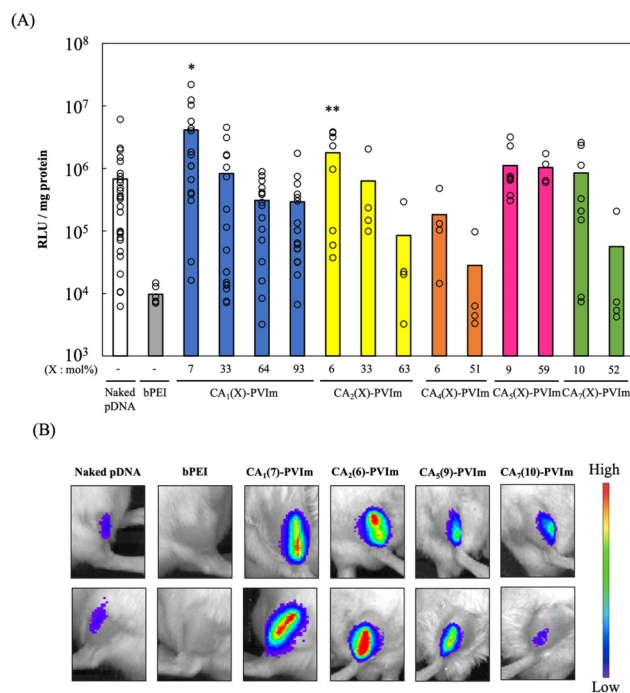


**Fig. 6** *In vivo* gene transfection efficiency in mouse skeletal muscles. (A) Luciferase gene expression by intramuscular injection of the CA-PVIm/pDNA PICs. The mixing charge ratios,  $[Im^+]_{CA-PVIm}/[R_2PO_4^-]_{pDNA}$ , are 64. Individual gene expression was determined relative light unit (RLU) normalized by the protein concentration. *P*-values are indicated: \**P* < 0.01, \*\**P* < 0.05 vs. naked pDNA. All data are represented as the mean and individual values (*n* = 4–28). (B) Representative images for *in vivo* gene expression. Using *in vivo* luciferase imaging system (IVIS), luciferase gene expression was observed in 1 week.

also decreased, when the methylene chain length of each CA-PVIm increased, presumably due to the increased length of the spacer between a cationic imidazolium group and an anionic carboxyl group, causing a reduced access to the anionic cellular membrane. Namely, the CA-PVIm/pDNA PICs with larger negative  $\zeta$ -potentials (Fig. 4B) were repelled by an anionic cellular membrane because it is reported that the surface coating of an anionic particle with albumin strongly reduces non-specific interactions with the plasma membrane as well as overall cell uptake.<sup>56</sup> As mentioned above, the  $\zeta$ -potentials of the CA-PVIm alone were negative (Fig. S8B†) in the presence of the imidazolium cations, supporting negligible interaction of negative cell walls with the imidazolium cations. Conversely, CM-PVIm zwitterionic polymers were formed under concentrated conditions ( $[\text{Im}^+]_{\text{CA-PVIm}}/[\text{R}_2\text{PO}_4^-]_{\text{pDNA}}$  ratio of 64), when the PICs between the CA-PVIm and pDNA were formed. Presumably, they interacted with the pDNA through their imidazolium cations.

One important factor for efficient pDNA delivery is the escape from endosomes and acidic intracellular vesicles because the above-mentioned negative  $\zeta$ -potentials (Fig. 4B) related to cell uptake<sup>56</sup> are not correlated with the resulting gene expression (Fig. 6A). Actually, the uptake efficiency of the CA<sub>1</sub>(7)-PVIm seems to be almost the same (or a little higher) than that of the other CA-PVIm PICs (Fig. S15A†) because of negligible gene transfection efficiency *in vitro* (Fig. S15B†). The proton sponge hypothesis is a promising mechanism for endosomal escape, where the PEI is typically used.<sup>57,58</sup> Imidazole heterocyclic rings with a  $\text{pK}_a$  of around 6 have a buffering capacity at endosomal pH, and the resulting protonation of the imidazole heterocyclic rings inside an endosome can exhibit a proton sponge effect. Indeed, the polymers modified with histidine or imidazole groups show significant enhancement in the pDNA gene expression as compared to unmodified polymers.<sup>59–63</sup> In this study, the CA-PVIm/pDNA PICs showed more retarded bands at endosomal pH (Fig. S13†), as compared to near physiological pH (Fig. 3). Especially, the complete retardation of the pDNA bands was observed by use of the CA-PVIm with a lower degree of CA group modification, suggesting the protonation of unmodified imidazole groups at endosomal pH.

Furthermore, the hemolytic activity at endosomal pH increased, as compared to physiological pH, in the presence of the CA-PVIm with a lower degree of CA group modification (Fig. S14†). Especially, the CA<sub>1</sub>(7)-PVIm exhibited significant ( $P < 0.05$ ) hemolysis as compared to CA<sub>1</sub>(93)-PVIm. The resulting hemolytic activity was almost correlated with gene expression mediated by the CA-PVIm/pDNA PICs (Fig. 6A). Namely, the highest gene expression was significantly ( $P < 0.01$ ) mediated by the CA<sub>1</sub>(7)-PVIm/pDNA PIC, as compared to the naked pDNA. These results suggest that the endosomal escape by the CA-PVIm with a lower degree of CA group modification is also attributed to higher gene expression because the pDNA is released from the PIC by competitive exchange with anionic proteins in the cytoplasm at physiological pH after the endosomal escape.<sup>64</sup>

Finally, we examined the gene expression in mouse skeletal muscles by *in vivo* luciferase imaging. Fig. 6B shows the resulting image of the CA-PVIm/pDNA PICs with a lower degree of CA group modification by use of IVIS. Each gene expression level was almost correlated with the relative light unit (RLU) value (Fig. 6A). Especially, it is worth noting that the area of gene expression seems to be the widest for the intramuscular injection of the CA<sub>1</sub>(7)-PVIm/pDNA PIC, as well as gene expression level. The resulting widespread area of the gene expression suggests that the CA<sub>1</sub>(7)-PVIm/pDNA PIC is effective for the diffusive delivery of the pDNA into the skeletal muscle for the treatment of serious muscle diseases, as compared to the naked pDNA. The skeletal muscles, such as a tibialis muscle, that are injected by the CA<sub>1</sub>(7)-PVIm/pDNA PIC are important for the motor function of the body, and thus, the diffusive delivery of the pDNA into a huge volume of the muscle is necessary for the treatment of serious muscle diseases. Owing to the diffusive delivery of the pDNA by the CA<sub>1</sub>(7)-PVIm, we are now trying the regeneration of skeletal muscles using the pDNA to express shRNAs delivered with CA<sub>1</sub>(7)-PVIm zwitterionic polymers.

## 4. Conclusion

The CA-PVIm zwitterionic polymers with the imidazolium cations and carboxylate anions have been synthesized as a carrier for the delivery of the pDNA into skeletal muscle. The result is the CA-PVIm with the intermediate water in the hydration water as a biocompatible polymer. Notably, when the pDNA and resulting CA-PVIm were mixed, slight retarded bands of the pDNA were observed in agarose gel electrophoresis, suggesting PIC formation between the pDNA and CA<sub>1</sub>-PVIm despite the presence of the zwitterionic polymer. The resulting PICs maintained the higher-order structure of the pDNA. Consequently, the highest pDNA expression by intramuscular injection was achieved in the CA<sub>1</sub>(7)-PVIm/pDNA PIC, which was observed in the widest area of skeletal muscle, suggesting a diffusive delivery of the pDNA into skeletal muscle for the treatment of serious muscle diseases.

## Author contributions

Ren Misaizu: investigation, methodology, writing – original draft. Yoko Endo-Takahashi: investigation, methodology. Kei Nirasawa: investigation, methodology. Yoichi Negishi: investigation, methodology. Shoichiro Asayama: conceptualization, supervision, validation, writing – original draft, writing – review & editing, visualization, funding acquisition.

## Ethical statement

All procedures involving animals were performed in accordance with the Guidelines for Care and Use of Laboratory Animals of Tokyo University of Pharmacy and Life Sciences

and approved by the Animal Ethics Committee of Animal Use and Welfare.

## Conflicts of interest

The authors declare no competing financial interest.

## Acknowledgements

This research was partially supported by a Grant-in-Aid for Scientific Research (B) from the Japan Society for the Promotion of Science (JSPS KAKENHI grant no. 21H03820). TEM observation was supported by the Center of the University of Tokyo for the Advanced Research Infrastructure for Materials and Data Hub (ARIM).

## References

- 1 S. M. Elbashir, J. Harborth, W. Lendeckel, A. Yalcin, K. Weber and T. Tuschl, *Nature*, 2001, **411**, 494–498.
- 2 S. Asayama, *Chem. Lett.*, 2020, **49**, 1–9.
- 3 R. M. Raftery, I. M. Castaño, G. Chen, B. Cavanagh, B. Quinn, C. M. Curtin, S. A. Cryan and F. J. O'Brien, *Biomaterials*, 2017, **149**, 116–127.
- 4 B. S. Rodrigues, H. Oue, A. Banerjee, T. Kanekiyo and J. Singh, *J. Controlled Release*, 2018, **286**, 264–278.
- 5 H. R. Phillips, Z. P. Tolstyka, B. C. Hall, J. K. Hexum, P. B. Hackett and T. M. Reineke, Hemocompatibility and In Vivo Biodistribution, *Biomacromolecules*, 2019, **20**, 1530–1544.
- 6 F. Lin, X. Shen, G. Kichaev, J. M. Mendoza, M. Yang, P. Armendi, J. Yan, G. P. Kobinger, A. Bello, A. S. Khan, K. E. Broderick and N. Y. Sardesai, *Hum. Gene Ther.: Methods*, 2012, **23**, 157–168.
- 7 E. K. Duperret, A. Trautz, R. Stoltz, A. Patel, M. C. Wise, A. Perales-Puchalt, T. Smith, K. E. Broderick, E. Masteller, J. J. Kim, L. Humeau, K. Muthumani and D. B. Weiner, *Cancer Res.*, 2018, **78**, 6363–6370.
- 8 S. Y. Kwak, H. D. Han and H. J. Ahn, *Sci. Rep.*, 2019, 2993.
- 9 S. A. Smith, L. I. Selby, A. P. R. Johnston and G. K. Such, *Bioconjugate Chem.*, 2019, **30**, 263–272.
- 10 W. A. Lackington, M. A. Gomez-Sierra, A. González-Vázquez, F. J. O'Brien, M. J. Stoddart and K. Thompson, *Front. Bioeng. Biotechnol.*, 2020, **8**, 582012.
- 11 M. Thomas and A. M. Klibanov, *Proc. Natl. Acad. Sci. U. S. A.*, 2003, **100**, 9138–9143.
- 12 S. S. Talsma, J. E. Babensee, N. Murthy and I. R. Williams, *J. Controlled Release*, 2006, **112**, 271–279.
- 13 A. I. S. van den Berg, C. O. Yun, R. M. Schiffelers and W. E. Hennink, *J. Controlled Release*, 2021, **331**, 121–141.
- 14 N. Pardi, S. Tuyishime, H. Muramatsu, K. Kariko, B. L. Mui, Y. K. Tam, T. D. Madden, M. J. Hope and D. Weissman, *J. Controlled Release*, 2015, **217**, 345–351.
- 15 R. Rai, S. Alwani and I. Badea, *Polymers*, 2019, **11**, 745.
- 16 R. E. Decker, Z. E. Lamantia, T. S. Emrick and M. L. Figueiredo, *Bioengineering*, 2020, **7**, 107.
- 17 D. Eusébio, A. R. Neves, D. Costa, S. Biswas, G. Alves, Z. Cui and Â. Sousa, *Drug Discovery Today*, 2021, **26**, 2575–2592.
- 18 L. Parhamifar, A. K. Larsen, A. C. Hunter, T. L. Andresen and S. M. Moghimi, *Soft Matter*, 2010, **6**, 4001–4009.
- 19 T. Nomoto, Y. Matsumoto, K. Miyata, M. Oba, S. Fukushima, N. Nishiyama, T. Yamasoba and K. Kataoka, *J. Controlled Release*, 2011, **151**, 104–109.
- 20 A. L. Klibanov, K. Maruyama, V. P. Torchilin and L. Huang, *FEBS Lett.*, 1990, **268**, 235–237.
- 21 H. Hatakeyama, H. Akita and H. Harashima, *Adv. Drug Delivery Rev.*, 2011, **63**, 152–160.
- 22 H. Hatakeyama, H. Akita and H. Harashima, *Biol. Pharm. Bull.*, 2013, **36**, 892–899.
- 23 H. Hatakeyama, H. Akita, K. Kogure, M. Oishi, Y. Nagasaki, Y. Kihira, M. Ueno, H. Kobayashi, H. Kikuchi and H. Harashima, *Gene Ther.*, 2007, **14**, 68–77.
- 24 T. Ishida, M. Ichihara, X. Y. Wang, K. Yamamoto, J. Kimura, E. Majima and H. Kiwada, *J. Controlled Release*, 2006, **112**, 15–25.
- 25 E. T. M. Dams, P. Laverman, W. J. G. Oyen, G. Storm, G. L. Scherphof, J. W. M. van der Meer, F. H. M. Corstens and O. C. Boerman, *J. Pharmacol. Exp. Ther.*, 2000, **292**, 1071–1079.
- 26 P. Laverman, M. G. Carstens, O. C. Boerman, E. T. M. Dams, W. J. G. Oyen, N. van Rooijen, F. H. M. Corstens and G. Storm, *J. Pharmacol. Exp. Ther.*, 2001, **298**, 607–612.
- 27 P. Laverman, O. C. Boerman, W. J. G. Oyen, F. H. M. Corstens and G. Storm, *Crit. Rev. Ther. Drug Carrier Syst.*, 2001, **18**, 551–566.
- 28 T. Ishida, R. Maeda, M. Ichihara, Y. Mukai, Y. Motoki, Y. Manabe, K. Irimura and H. Kiwada, *Cell. Mol. Biol. Lett.*, 2002, **7**, 286.
- 29 T. Ishida, R. Maeda, M. Ichihara, K. Irimura and H. Kiwada, *J. Controlled Release*, 2003, **88**, 35–42.
- 30 T. Ishida, K. Masuda, T. Ichikawa, M. Ichihara, K. Irimura and H. Kiwada, *Int. J. Pharm.*, 2003, **255**, 167–174.
- 31 T. Ishida, T. Ichikawa, M. Ichihara, Y. Sadzuka and H. Kiwada, *J. Controlled Release*, 2004, **95**, 403–412.
- 32 J. Szebeni, *Mol. Immunol.*, 2014, **61**, 163–173.
- 33 L. Y. Zhou, Y. H. Zhu, X. Y. Wang, C. Shen, X. W. Wei, T. Xu and Z. Y. He, *Comput. Struct. Biotechnol. J.*, 2020, **18**, 1980–1999.
- 34 W. Yang, S. Liu, T. Bai, A. J. Keefe, L. Zhang, J. R. Ella-Menye, Y. Li and S. Jiang, *Nano Today*, 2014, **9**, 10–16.
- 35 Y. Li, R. Liu, Y. Shi, Z. Zhang and X. Zhang, *Theranostics*, 2015, **5**, 583–596.
- 36 S. Asayama, H. Kato and H. Kawakami, *Polym. Adv. Technol.*, 2007, **18**, 329–333.
- 37 S. Asayama, M. Sudo, S. Nagaoka and H. Kawakami, *Mol. Pharmaceutics*, 2008, **5**, 898–901.
- 38 S. Asayama, K. Seno and H. Kawakami, *Chem. Lett.*, 2013, **42**, 358–360.
- 39 J. Gu, X. Wang, X. Jiang, Y. Chen, L. Chen, X. Fang and X. Sha, *Biomaterials*, 2012, **33**, 644–658.



- 40 J. Gu, X. Chen, H. Xin, X. Fang and X. Sha, *Int. J. Pharm.*, 2014, **461**, 559–569.
- 41 J. Zhang, Z. Wang, W. Lin and S. Chen, *Biomaterials*, 2014, **35**, 7909–7918.
- 42 K. M. Dave, L. Han, M. A. Jackson, L. Kadlecik, C. L. Duvall and D. S. Manickam, *Pharm. Res.*, 2020, **37**, 176.
- 43 H. Lv, S. Zhang, B. Wang, S. Cui and J. Yan, *J. Controlled Release*, 2006, **114**, 100–109.
- 44 R. Kamboj, S. Sukhprit, A. Bhadani, H. Kataria and G. Kaur, *Langmuir*, 2012, **28**, 11969–11978.
- 45 S. K. Misra, M. Muñoz-Úbeda, S. Datta, A. L. Barrán-Berdón, C. Aicart-Ramos, P. Castro-Hartmann, P. Kondaiah, E. Junquera, S. Bhattacharya and E. Aicart, *Biomacromolecules*, 2013, **14**, 3951–3963.
- 46 J. M. Unsworth, F. R. A. J. Rose, R. E. Wright, C. A. Scotchford and K. M. Shakesheff, *J. Biomed. Mater. Res.*, 2003, **53**, 617–620.
- 47 Y. Negishi, K. Matsuo, Y. Endo-Takahashi, K. Suzuki, Y. Matsuki, N. Takagi, R. Suzuki, K. Maruyama and Y. Aramaki, *Pharm. Res.*, 2011, **28**, 712–719.
- 48 M. Tanaka, T. Motomura, N. Ishii, K. Shimura, M. Onishi, A. Mochizuki and T. Hatakeyama, *Polym. Int.*, 2000, **49**, 1709–1713.
- 49 M. Tanaka and A. Mochizuki, *J. Biomater. Sci., Polym. Ed.*, 2010, **21**, 1849–1863.
- 50 T. Hatakeyama, M. Tanaka and H. Hatakeyama, *Acta Biomater.*, 2010, **6**, 2077–2082.
- 51 C. W. Pouton, P. Lucas, B. J. Thomas, A. N. Uduehi, D. A. Milroy and S. H. Moss, *J. Controlled Release*, 1998, **53**, 289–299.
- 52 Q. Shao and S. Jiang, *J. Phys. Chem. B*, 2013, **117**, 1357–1366.
- 53 Y. Kobayashi, K. Nirasawa, Y. Negishi and S. Asayama, *J. Biomater. Sci., Polym. Ed.*, 2021, **32**, 405–416.
- 54 R. Morishita, M. Aoki, N. Hashiya, H. Makino, K. Yamasaki, J. Azuma, Y. Sawa, H. Matsuda, Y. Kaneda and T. Ogihara, *Hypertension*, 2004, **44**, 203–209.
- 55 H. Shigematsu, K. Yasuda, T. Iwai, T. Sasajima, S. Ishimaru, Y. Ohashi, T. Yamaguchi, T. Ogihara and R. Morishita, *Gene Ther.*, 2010, **17**, 1152–1161.
- 56 C. Wilhelm, C. Billotey, J. Roger, J. N. Pons, J. C. Bacri and F. Gazeau, *Biomaterials*, 2003, **24**, 1001–1011.
- 57 O. Boussif, F. Lezoualc'h, M. A. Zanta, M. D. Mergny, D. Scherman, B. Demeneix and J. P. Behr, *Proc. Natl. Acad. Sci. U. S. A.*, 1995, **92**, 7297–7301.
- 58 N. D. Sonawane, F. C. Szoka Jr and A. S. Verkman, *J. Biol. Chem.*, 2003, **278**, 44826–44831.
- 59 M. B. Roufaï and P. Midoux, *Bioconjugate Chem.*, 2001, **121**, 92–99.
- 60 T. H. Kim, J. E. Ihm, Y. J. Choi, J. W. Nah and C. S. Cho, *J. Controlled Release*, 2003, **93**, 389–402.
- 61 J. S. Park, T. H. Han, K. Y. Lee, S. S. Han, J. J. Hwang, D. H. Moon, S. Y. Kim and Y. W. Cho, *J. Controlled Release*, 2006, **115**, 37–45.
- 62 S. Mishra, J. D. Heidel, P. Webster and M. E. Davis, *J. Controlled Release*, 2006, **116**, 179–191.
- 63 A. Swami, A. Aggarwal, A. Pathak, S. Patnaik, P. Kumar, Y. Singh and K. C. Gupta, *Int. J. Pharm.*, 2007, **335**, 180–192.
- 64 C. Chittimalla, L. Zammuto-Italiano, G. Zuber and J. P. Behr, *J. Am. Chem. Sci.*, 2005, **127**, 11436–11441.